JOURNAL OF OPTOELECTRONICS AND ADVANCED MATERIALS Vol. 8, No. 6, December 2006, p. 2148 - 2155

Nonlinear properties of chalcogenide glass fibers

J. S. SANGHERA, I. D. AGGARWAL, L. B. SHAW, C. M. FLOREA[a],
P. PUREZA, V. Q. NGUYEN, F. KUNG, I. D. AGGARWAL
Naval Research Laboratory, Code 5606, Washington, DC 20375, USA
[a]SFA Inc., Crofton, MD 21114
[2]UMD Research Foundation, Greenbelt, MD 20770

Chalcogenide glasses have demonstrated high third-order Kerr ($\chi^{(3)}$) nonlinearities up to 1000x higher than silica glass which make them attractive for applications such as nonlinear switching, optical regeneration, Raman amplification, parametric amplification, and supercontinuum generation. Poling of chalcogenide glasses to induce an effective second order ($\chi^{(2)}$) nonlinearity has also been demonstrated and opens the possibility for the use of poled glass waveguides for applications such as frequency conversion or electro-optic modulation. Stimulated Brillouin scattering (SBS) has also been investigated in As_2S_3 and As_2Se_3 single-mode fibers. The threshold intensity for the stimulated Brillouin scattering process was measured and used to estimate the Brillouin gain coefficient. Preliminary results indicate record high values for the figure of merit and theoretical gain, compared to silica, which bodes well for slow-light based applications in chalcogenide fibers.

(Received November 7, 2006; accepted November 8, 2006)

Keywords: Chalcogenide Glass, Optical fibers, Nonlinear properties

1. Introduction

Chalcogenide glasses are based on the chalcogen elements S, Se and Te with the addition of other elements such as Ge, As and Sb to form of stable glasses [1]. Due to their large IR transparency, fibers fabricated from these glasses are ideal for transmission of high power IR light. Several applications of chalcogenide fibers for IR transmission have been documented [2]. Also of interest is the high nonlinearity of these glass compositions. The high $\chi^{(3)}$ nonlinearities of chalcogenide glasses make them excellent candidates for applications such as all nonlinear switching, optical regeneration, Raman amplification, parametric amplifiers and supercontinuum generation. We have extensively studied the nonlinearities of the As-S-Se based system. High strength low loss fibers can be drawn from this system. In this paper, we will report on the nonlinear properties of this system.

2. Glass preparation

Chalcogenide glasses are melted directly in quartz ampoules using chemicals purified via distillation/sublimation [3]. Typical melt temperatures range from 600°C to 900°C, depending upon composition. The liquids are quenched and the glass rods annealed at temperatures around the appropriate softening temperatures. The optical fibers are obtained by the double crucible (DC) process [4]. The DC process enables adjustments to be made in the core/clad diameter ratio during fiber drawing by independent pressure control above each melt. Therefore both multimode and single mode fibers can be drawn with relatively few processing steps.

3. Fiber properties

Fig. 1 compares the losses routinely obtained for a couple of chalcogenide glasses along with the lowest ("champion") losses reported in the literature [5,6]. Depending upon composition, the sulfide, selenide and telluride based fibers transmit between about 0.8-7 μm, 1-10 μm, and 2-12 μm, respectively. Therefore, the practical applications dictate the type of fiber to be used. The As-S fibers have received the most attention to-date in our laboratory and so the loss routinely achieved is about 0.1-0.2 dB/m in fiber lengths of about 500 meters. Losses for As-Se fibers typically range from 0.5 to 1 dB/m in the near IR around 1.5 μm.

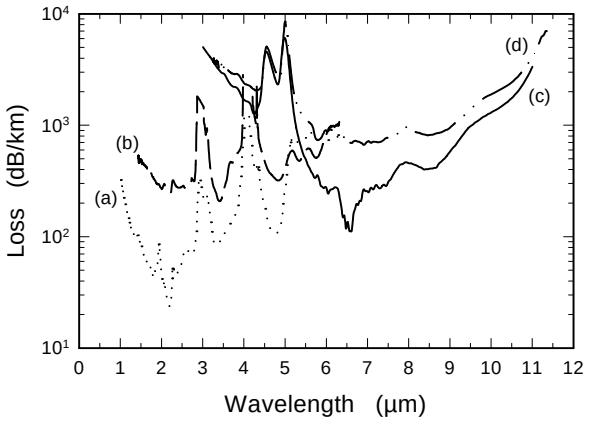

Fig. 1. Transmission loss spectra of (a) lowest loss sulfide fiber, (b) typical sulfide fiber, (c) lowest loss telluride fiber, and (d) typical telluride fiber.

4. Nonlinear properties

It is well established that the values of $\chi^{(3)}$ for chalcogenide glasses are about two orders of magnitude larger than silica [7,8]. More recently, glasses have been reported with non-linearities approaching 1000 times silica [9,10]. These large nonlinearities would allow small compact low power devices for telecommunications. The subpicosecond response or these nonlinearities is ideal for high data rate telecommunication devices.

For efficient nonlinear switches utilizing the optical Kerr effect, the nonlinearity must be high and the nonlinear absorption must be low. A figure of merit FOM – $n_2/(\beta\lambda)$ can be defined as a useful metric to determine optimum compositions, where n_2 is the nonlinear index and β is the nonlinear absorption. For isotropic medium, one and two photon resonant processes dominate the third-order susceptibility. For frequencies approximately half of the material resonance, two photon processes resonantly enhance the nonlinear index n_2. Normally, however, the two photon resonance enhancement is accompanied by two photon absorption which competes with the nonlinear index n_2. In the case of amorphous materials such as chalcogenide glass, an exponential Urbach tail exists and its absorption edge extends below the half gap. This edge leads to two photon absorption (TPA) below the half gap and thus n_2 may increase faster than TPA absorption in this region. Consequently, we expect to find that the best performance in terms of nonlinear index strength vs. TPA (FOM) will occur just below the gap. Fig. 2 shows the bandgap of the As-S-Se system vs. Se concentration.

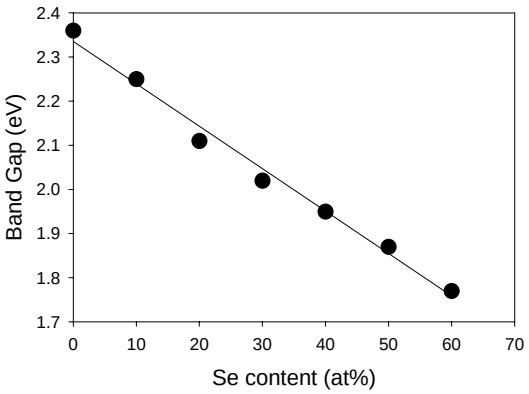

Fig. 2. Bandgap of As-S-Se glass system. Bandgap is defined at the point of 10^3 cm^{-1} absorption

Here, the bandgap is defined at the point of 10^3 cm^{-1} absorption. In the graph, Se content of 0 at. % corresponds to pure $As_{40}S_{60}$ while Se content of 60 at. % corresponds to pure $As_{40}Se_{60}$. We note that the bandgap of glass system increases with Se content. For operation at 1.55 μm (0.8 eV), we would expect an optimum composition of $As_{40}Se_{60}$ where $E_g/h\nu \sim 0.45$. We will see that this is borne out by experimental data.

Spectrally resolved two beam coupling measurements of As-S-Se system have been formed to determine the magnitude of the nonlinear index n_2 and the two photon absorption coefficient. Details of these measurements can be found in [10]. Fig. 3 shows the results of these measurements. Values for As-S were found to be ~220 times silica at 1.55 μm and increased with Se substitution of S to a value of ~930 times silica for As-Se. Likewise, two photon absorption also increases with increasing Se content. We can use this data to calculate the FOM for the As-Se system (Fig. 4). As expected. The glasses with the larges FOM for operation at 1550 nm occurs for $E_g/h\nu$ at ~0.45 which is the As-Se composition. [11]

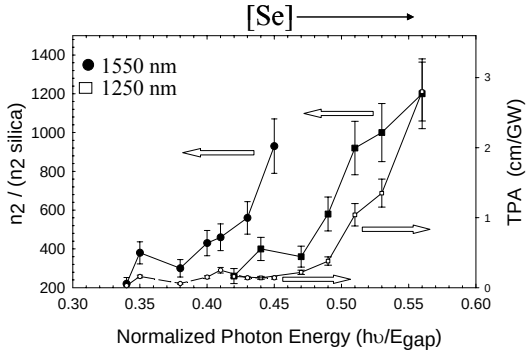

Fig. 3. n_2 and TPA absorption of As-S-Se glass system.

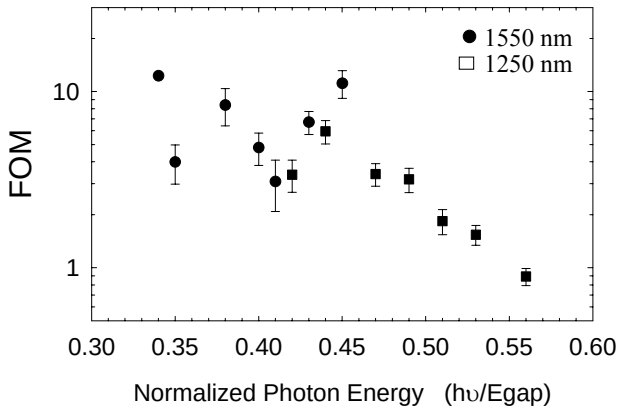

Fig. 4. FOM for As-S-Se glass system.

5. Raman amplification

Fig. 5 shows the normalized Raman spectra of $As_{40}S_{60}$, $As_{40}Se_{60}$, and silica. $As_{40}Se_{60}$ glass has a much narrower Raman line (~60 cm^{-1}) than silica glass (~250 cm^{-1}). In addition, the Raman shift for $As_{40}Se_{60}$ glass is much smaller (~240 cm^{-1}) than the Raman shift of silica glass (~440 cm^{-1}) due to the heavier atoms present in the chalcogenide glass. Previous studies have looked at stimulated Raman scattering in $As_{40}S_{60}$ glass, a very similar glass system to $As_{40}Se_{60}$ [12]. These studies found the Raman gain coefficient of $As_{40}S_{60}$ to be almost two orders of magnitude higher than that of silica. It was also

found that this enhancement in the Raman gain roughly corresponded to the enhancement in the nonlinear index, n_2. Consequently, one might expect to see an even larger Raman gain coefficient in $As_{40}Se_{60}$ since the selenide glass has shown an even larger nonlinearity and also a narrower Raman spectrum.

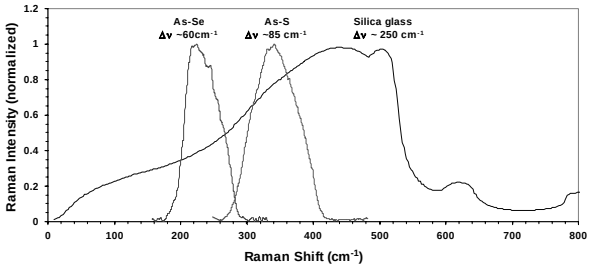

Fig. 5. Raman spectra of As_2S_3 and As_2Se_3 glass. Silica glass is shown for reference.

We have demonstrated Raman amplification at 1.55 μm in small core As-Se fiber [13]. The result of the Raman amplification experiment are shown in shown in Figure 6. We observed over ~23 dB of gain in a 1.1-meter length of fiber pumped by a nanosecond pulse of ~10.8 W peak power at 1.50 μm. The peak of the Raman gain was shifted by ~230 cm^{-1} to 1.56 μm. The Raman gain coefficient was estimated to be ~300 times silica in this experiment. More recent measurements of the Raman gain coefficient show a value of about 780x greater than that of silica [11].

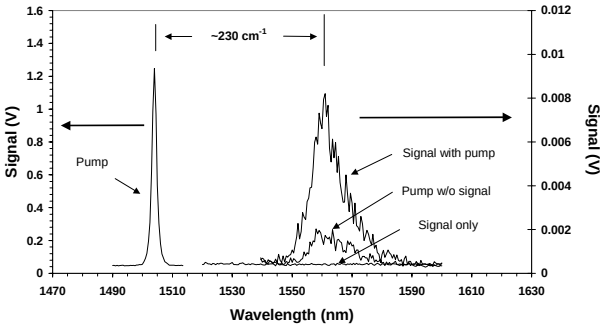

Fig. 6. Raman amplification in As-Se fiber. Shown is amplifier output with signal and no pump, pump and no signal (showing background stimulated Raman scattering (SRS) resulting from pump), and amplified signal with pump.

The large Raman gain coefficient of chalcogenide glass coupled with its large IR transparency show promise for lasers and amplifiers in the near and mid-IR. We can assess the potential for Raman lasers and amplifiers by defining a figure of merit (FOM). The expression for single pass gain, G_A, in a Raman fiber laser is given by [11]

$$G_A = \exp\left(\frac{g_R P_0 L_{eff}}{A_{eff}}\right) \quad (1)$$

Where g_R is the Raman gain coefficient, P_0 is the pump power, A_{eff} is the fiber effective area and L_{eff} is the fiber effective length. The fiber effective length is given by

$$L_{eff} = \frac{1}{\alpha}\left(1 - e^{-\alpha \cdot L}\right) \approx \frac{1}{\alpha} \quad (2)$$

Where α is the fiber loss. For long lengths, L_{eff} is approx $1/\alpha$. From these equations, we can see that the gain is proportional to *exp* $(-g_R/\alpha)$ for long fiber lengths. Thus, we can use the value g_R/α as a rough FOM for Raman amplification. Table 1 compares the performance of an As-Se Raman fiber laser or amplifier operating at 4 μm to a silica Raman fiber laser or amplifier operating in the telecommunications band at 1.5 μm. Here, the Raman gain coefficient of As-Se, g_R, which is measured to be 780x silica at 1.5 μm is extrapolated to it value in the mid-IR since the Raman gain coefficient scales inversely with wavelength. α is the fiber loss. For silica, a loss of 0.2 to 0.3 dB/km is typical of telecommunication grade fiber. For As-Se, two losses are given. The loss of 200 dB/km is typical of "champion losses" achieved at NRL for As-Se fiber while the loss of 0.1 dB/km is theoretical loss for As-Se fiber [14]. For the loss of 200 dB/km, we see that g_R/α for an As-Se fiber Raman amplifier operating at 4 μm is about 0.38 compared to 1.1 for a silica fiber Raman amplifier. For the theoretical loss of 0.1 dB/km, we see that g_R/α for As-Se fiber operating at 4 μm is 860 times that of silica fiber operating at 1.5-μm.

Table 1. Figure of merit for Raman amplification in As-Se fiber at 4-μm compared Raman amplification in silica fiber at 1.5-μm. The loss value of 200 dB/km (a) for As-Se is typical of a "champion" loss value. The loss value of 0.1 dB/km (b) is theoretical loss from [14].

	λ (μm)	g_R (cm/W)	Loss (dB/km)	α (cm^{-1})	g_R/α ($10^{-6}W^{-1}$)
Silica Fiber	1.5	0.65×10^{-12}	0.2-0.3	~6×10^{-7}	1.1
As-Se Fiber	4	1.9×10^{-10}	200(a)	5×10^{-4}	0.38
			0.1(b)	2×10^{-7}	950

Stimulated Raman scattering (SRS) has also been observed in the IR. Fig. 7 shows the SRS in a ~ 1m length of As-Se fiber under CW CO laser pumping at ~ 5.4 μm. The SRS is seen at ~ 6.1 μm. Raman laser operating in the wavelength range of from 6.1 to 6.4 μm would have applications in laser surgery. These wavelengths correspond to amide II bands in tissues and studies have shown that ablation of soft tissue is possible at these wavelengths with minimal collateral damage, thus accelerating healing [15]. Modeling of a Raman laser operating at 6.45 μm under CO laser pumping at 5.59 μm has shown high slope efficiencies and moderate threshold power operation is possible [16]

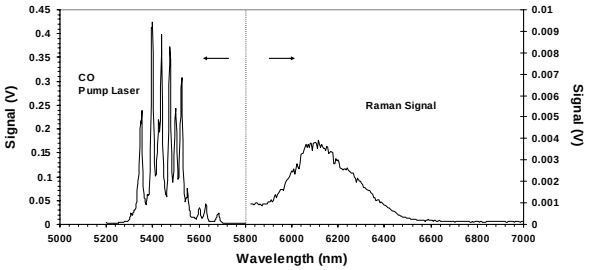

Fig. 7. SRS signal observed at 6.1 μm under ~5.4 μm CO laser pumping.

6. Supercontinuum generation

Supercontinuum generation has been demonstrated for between 2 to 3 μm in small core sulfide and selenide fibers as well as photonic crystal selenide fibers [17]. The 1 meter length of fibers were pumped with a Ti:sapphire laser at a wavelength of 2.5 μm using 100 fs pulses and 100 pJ/pulse. The outputs from the fibers are shown in figure 5. The sulfide and selenide fibers were 7 μm core diameter, while the PCF fiber had a 10 μm core diameter.

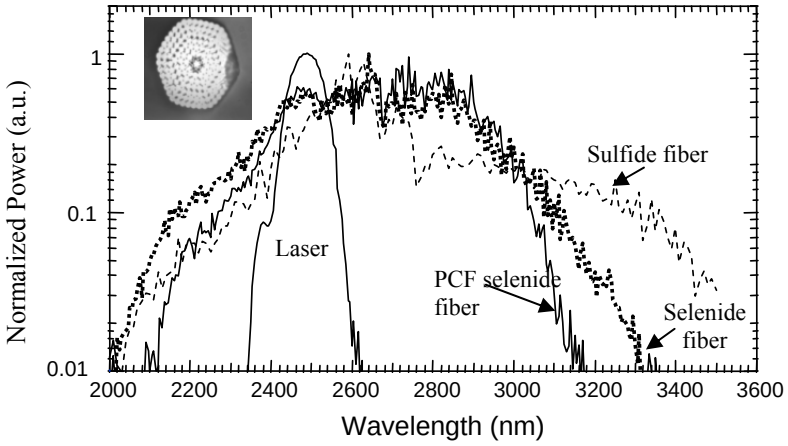

Fig. 8. Supercontinuum generation in small core chalcogenide fibers. The insert shows the cross-sectional view of the selenide PCF fiber.

Broader supercontinuum can be realized by pumping near to the zero dispersion wavelength or in the anomalous dispersions region. Currently, however, pumping is limited by the tuning range of the OPA-800C to ~2500 nm wavelength. Tailoring the dispersion of the As-Se PCF fiber to shift the dispersion wavelength closer to the near IR to enable broader bandwidth supercontinuum is feasible. Work on chalcogenide PCF fiber has shown that that the minimum dispersion wavelength can be shifted over very broad ranges [17].

7. Poling of chalcogenide glass

Isotropic materials such as glasses lack a center of inversion symmetry and thus have no second order nonlinear susceptibility ($\chi^{(2)}$) they should not exhibit second harmonic generation (SHG) [18]. However, undoped and Pr-doped GaLaS glasses have exhibited SHG [19] through optical pumping. This SHG may be due to crystallization or the effect of frozen-in electric fields. The latter arises from the relationship $\chi^{(2)} = E_{dc}\chi^{(3)}$, where E_{dc} is the frozen-in electric field [18]. Electric poling has been successfully used to produce SHG in silica based fiber systems [20]. It is not unreasonable to expect similar results in chalcogenide fibers.

Since $\chi^{(3)}$ is about 2 to 3 orders of magnitude larger in chalcogenides compared with silica, we expect larger SHG efficiencies in electrically poled chalcogenide glasses. However, the question arises as to whether the electric fields can be frozen-in for chalcogenide glasses. We have observed second harmonic generation at 780 nm using electrically poled arsenic sulfide glass when pumping a 1 mm thick arsenic sulfide glass disk at 1560 nm. The sample was electrically poled at 100°C for 5 hours under nitrogen gas atmosphere. At the present time the magnitude appears comparable to silica glass but the mechanism is unknown.

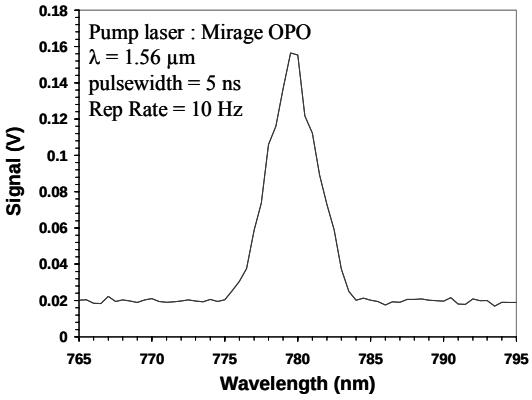

Fig. 9. Second harmonic generation in poled As-S glass. Glass was pumped at 1.56 μm. Shown is 780 nm SHG signal.

8. Brillouin scatteing

In order to determine the Brillouin gain coefficient, we measured the threshold power of the stimulated Brillouin scattering (SBS) process using the experimental setup detailed below in Fig. 10. The threshold power is easily determined by monitoring the spectrum of the reflected light using a high-resolution optical spectrum analyzer (OSA) as sampled by the circulator which is the interface between the pump delivery system (DFB laser source plus Er amplifier, EDFA) and the chalcogenide fiber. The fiber was coated with liquid gallium on 10-cm lengths on each end to eliminate the radiation leaking into the cladding. The fiber ends were not anti-reflection coated and hence cavity effects were significant due to the high refractive index of the fiber. The losses in the fiber, and the coupling optics (4% for the focusing lens, 14% for the collimating objective), along with the Fresnel loss at the fiber ends (17.7% for As_2S_3 and 22.6% for As_2Se_3) are all taken into account in throughput measurements used to estimate the coupling efficiency, and hence the amount of pump launched into the core. We estimate 45% coupling efficiency in the As_2S_3 case, and 37% in the As_2Se_3 case. In the future, the coupling efficiency can be optimized and hence the SBS threshold power can be reduced, which is a desired trend from a system design perspective.

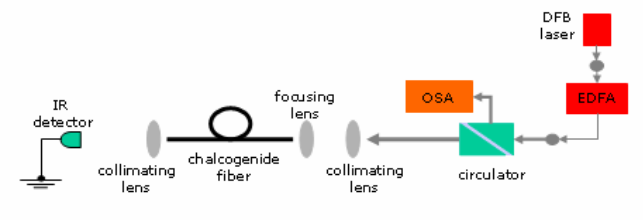

Fig. 10. Experimental setup used for SBS threshold measurements.

The spectral changes of the backward wave propagating through the chalcogenide fiber, as sampled by the circulator, are shown in Fig. 11 for the As_2S_3 fiber, and in Fig. 12 for the As_2Se_3 fiber. The cavity effects reduced the accuracy with which we were able to determine the threshold as indicated in the captions. Nevertheless, the threshold is easily identified by the significant jump in the peak of the Brillouin-shifted signal monitored on the OSA. Additionally, we observed clamping of the pump output power as, once the threshold is reached, most of the pump power is transferred to the Stokes wave [21].

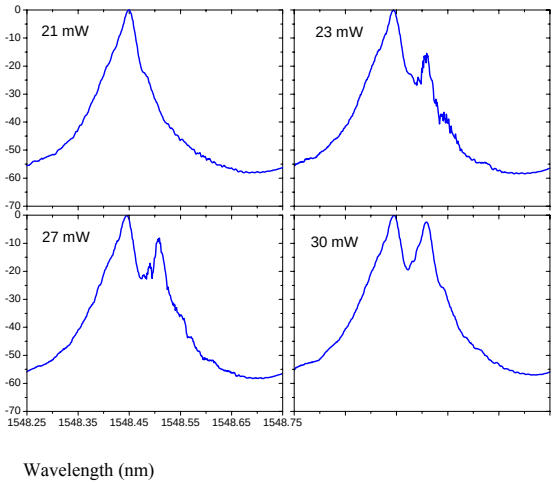

Fig. 11. Typical spectra of the reflected light sampled by the circulator for different launched pump powers into the As_2S_3 fiber core. Fiber length was 10.0 m. Estimated SBS threshold: (27 ± 3) mW. Tick labels shown only on one plot for clarity.

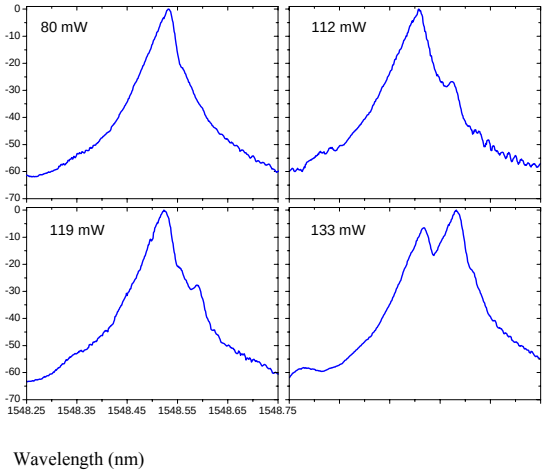

Fig. 12. Typical spectra of the reflected light sampled by the circulator for different launched pump powers into the As_2Se_3 fiber core. Fiber length was 5.0 m. Estimated SBS threshold: (127 ± 7) mW. Tick labels shown only on one plot for clarity.

The numerical aperture (NA) of a fiber, essentially the contrast in index between the core and the clad, is an important parameter. It determines the mode-field diameter and hence the effective area of the fundamental mode, with direct implications on the threshold power estimation for stimulated Brillouin scattering. It also determines the number of modes supported by the fiber at a given wavelength, λ. The V-number for a step-index fiber is a function of NA as given in Eq. 2, where d is the core diameter:

$$V = \frac{\pi d}{\lambda} NA \quad (3)$$

A value of V=2.405, or lower, indicates single mode behavior. Larger values indicate the potential for propagation of a higher number of modes. The V-number of ~2.8 for the As_2S_3 fiber suggests a second mode could be excited at 1.56 μm. In practice, the second mode was not observed. During the experiments, nevertheless we monitored the mode field pattern by imaging the output on a vidicon camera to make sure we launched only in the fundamental mode. Using the NA and V-number values, the Mode Field Diameter (MFD), $d_{1/e}{}^2$, for the fundamental mode will be given by Eq. 3 [12] and is listed in Table 2:

$$d_{1/e^2} = d \times (0.65 + \frac{1.619}{V^{1.5}} + \frac{2.879}{V^6}) \quad (4)$$

The propagation loss is also an important parameter as it defines the effective interaction length for the Brillouin scattering process. The values reported in Table 2 represent relatively low losses reported for both single mode fibers at 1.56 μm. However, it should be possible to lower the losses by improved fiber drawing and glass fabrication processes.

Table 2. Chalcogenide fiber parameters (at wavelength of 1.56 μm).

Fiber	Core dia. [μm]	Clad dia. [μm]	Core Refractive Index	NA	V-number	$1.e^{-2}$ MFD [μm] (calculated)	Loss [$dB.m^{-1}$]
As_2S_3	4.2	142.0	2.45	0.33	2.8	4.2	0.57
As_2Se_3	6.5	175.0	2.81	0.14	1.8	9.0	0.90

From the experimentally determined threshold power values (Pth) shown in figures 11 and 12, one can estimate the Brillouin gain coefficient (g_B) using Eq. 4 [22,23]:

$$P_{th} \cong 21 \frac{A_{eff}}{L_{eff} g_B k} \quad (5)$$

In the Eq. 4, k is a constant which reflects whether the polarization is maintained constant throughout the interaction (k = 1) or not (k = 0.5, our case). Also, the Aeff and Leff are the effective area of the fundamental mode, and the effective interaction length, respectively. These are given by Eq. 5 and Eq. 6, where L is the fiber length, α is the propagation loss, and the mode-field diameter is determined by Eq. 3 above.

$$A_{eff} = \frac{\pi d_{1/e^2}^2}{4} \quad (6)$$

$$L_{eff} = \frac{1}{\alpha}\left(1 - e^{-\alpha L}\right) \quad (7)$$

Using Eqs. 4-6, the parameters from Table 2, and the fiber lengths and pump threshold values indicated in Fig. 3 and Fig. 4, we determined the Brillouin coefficient to be $(3.9 \pm 0.4) \times 10^{-9}$ $m.W^{-1}$ for the As_2S_3 and $(6.75 \pm 0.35) \times 10^{-9}$ $m.W^{-1}$ for As_2Se_3. The value for the As_2Se_3 is close to the only other previously published result for this composition [22]. The value for the As_2S_3 fiber, although lower than the one for As_2Se_3, is still two orders of magnitude higher than that for fused silica ($\sim 4.4 \times 10^{-11}$ $m.W^{-1}$) [22,24].

The very large Brillouin gain coefficient presents the chalcogenide fibers as alternatives to silica fiber for slow-light applications. A figure of merit (FOM) has been proposed [22] in order to quantify the usefulness of a given fiber for slow-light based applications. The Brillouin gain is considered a positive factor while the length, the refractive index, and the power are considered as negative factors impacting the response time and the onset of additional nonlinear effects in the system. The FOM as defined in reference 22 requires knowledge of the actual Brillouin gain which has to be measured, and takes into account the effective length not the total length of fiber. We can re-write the FOM such as to reduce it to the primary quantities describing the fiber (effective area, length and propagation loss, refractive index, and Brillouin gain coefficient expressed in dB):

$$FOM \equiv \frac{Gain[dB]}{P_p n L} = \frac{10 \times \log(\exp(g_B k \frac{P_p}{A_{eff}} L_{eff}))}{P_p n L} \quad (8)$$

It is obvious that the FOM can be further reduced to:

$$FOM = 4.34 \frac{g_B k L_{eff}}{n A_{eff} L} \quad (9)$$

It is important to keep in mind that this FOM essentially determines what length and power are needed in a system to achieve a certain gain, and hence a certain time delay. The FOM as defined above in Eq. 8 tends to be a quantity which obscures the physical meaning contained in Eq. 7. Actually, the theoretical gain (G_{th}), expressed in dB, as given by Eq 6, could be used instead to compare different fibers, if one considers a standard fiber length of

1 m and a standard pump power of 1 mW. Then, the theoretical gain is given by Eq. 9:

$$G_{th}[dB] = 4.34 \frac{g_B k \times 1mW \times L_{eff}\big|_{L=1m}}{A_{eff}} \quad (10)$$

We used this last, fairly simple expression to compare the most representative fibers considered so far: silica [25,26], high-nonlinearity bismuth fiber [27,28], As_2Se_3 fiber [22], along with the results reported here. The comparison is provided in Table 3, with all the data reported for experiments without polarization control (k=0.5). We also include the FOM as defined above for completion. One can easily notice the significant increase in the theoretical gain (or FOM) for the As_2S_3 fiber due to its smaller core, lower loss and slightly reduced refractive index.

Table 3. Comparison of figure of merit for slow-light based applications at 1.56 μm.

	Silica [25,26]	Bi-HNL [27]	As_2Se_3 [22]	As_2Se_3	As_2S_3
n	1.47	2.22	2.81	2.81	2.45
Aeff [m^2]	$6.78x10^{-11}$	$0.3x10^{-11}$	$3.94x10^{-11}$	$6.31x10^{-11}$	$1.39x10^{-11}$
loss [$dB.m^{-1}$]	0.001	0.91	0.84	0.90	0.57
L [m]	2.0	2.0	5.0	5.0	10.0
Leff [m]	2.0	1.63	3.23	3.1	5.6
g_B [$m.W^{-1}$]	$4.40x10^{-11}$	$6.43\ x10^{-11}$	$6.10x10^{-9}$	$6.75x10^{-9}$	$3.90x10^{-9}$
G_{th} [dB]	0.076	0.003	1.084	0.719	3.398
FOM [$dB.W^{-1}.m^{-1}$]	1	17	77	51	139

9. Conclusions

The large nonlinearities and fast response of the nonlinearity of the As-S-Se system make fibers drawn from these glasses well suited for optical switches, optical regenerators for high speed telecommunication systems. Use of these materials will allow compact devices cm's in length with optical powers <1W peak power (1 pJ in 1 ps pulses). The large Raman gain of the As-S-Se fibers coupled with the large IR transparency make these well suited for compact Raman amplifiers for telecommunications as well as fiber lasers and amplifiers in the mid-IR. These high nonlinearities also allow efficient supercontinuum generation which is useful for broadband sources in the near and mid-IR. Finally these materials can be poled to induce an effective $\chi^{(2)}$, opening up the potential of waveguide parametric amplifiers.

The stimulated Brillouin scattering process was studied in As_2S_3 and As_2Se_3 single mode fibers. Values of the Brillouin gain coefficient were measured to be $(3.9 \pm 0.4) \times 10^{-9}$ $m.W^{-1}$ and $(6.75 \pm 0.35) \times 10^{-9}$ $m.W^{-1}$, respectively. An analysis of the figure of merit for slow-light based applications indicates that the smaller core As_2S_3 fiber performs best due to the lower loss, reduced core size and slightly lower refractive index. The configuration using the small-core As_2S_3 fiber yields a figure of merit which is about 140 times larger, or a theoretical gain about 45 times larger, than the best silica-based configurations reported to date.

The continued improvement of chalcogenide materials will make such devices feasible in the near term.

References

[1] Z. U. Borisova, Glassy Semicondutors, Plennum Press, NY 1981.

[2] J. S. Sanghera, I. D. Aggarwal, L. E. Busse, P. C. Pureza, V. Q. Nguyen, F. H. Kung, L. B. Shaw, F. Chenard., Chalcogenide Optical Fibers Target Mid-IR Applications, Laser Focus World, April **41** (4), 83 (2005).

[3] J. S. Sanghera, L. E.Busse, I. D. Aggarwal, J. Appl. Phys. **75**, 4885 (1994).

[4] J. S. Sanghera, I. D. Aggarwal, L. Busse, P. Pureza, V. Nguyen, R. Miklos, F. Kung, R. Mossadegh, SPIE, **2396**, 71 (1995).

[5] J. S. Sanghera, V.Q. Nguyen, P. C. Pureza, F. H.Kung, R. Miklos, I. D. Aggarwal, J. Lightwave Tech., **12**, 737 (1994).

[6] M. F. Churbanov, J. Non-Cryst. Solids **140**, 324 (1992).

[7] H. Nasu, Y. Ibara, K. Kubodera, J. Non-Cryst. Solids **110**, 229 (1989).

[8] K. A.Richardson, J. M. McKinley, B. Lawrence, S. Joshi, A. Villeneuve, Opt. Mats. **10**, 155 (1998).

[9] G. Lenz, J. Zimmermann, T. Katsufuji, M. E. Lines, H. Y. Hwang, S. Spalter, R. E. Slusher, S. W. Cheong, J. S. Sanghera, I. D. Aggarwal, Optics Letts. **25**, 254 (2000).

[10] J. M. Harbold, F. Ö. Ilday, F. W. Wise, J. S. Sanghera, V. Q. Nguyen, L. B. Shaw, I. D. Aggarwal, Optics Letters **27**, 119 (2002).

[11] R. E. Slusher, J. Hodelin, J. S. Sanghera, L. B. Shaw I. D. Aggarwal, JOSA-B **21**, 1146 (2004).
[12] M. Asobe, T. Kanamori, K. Naganuma, H. Itoh, T. Kaino, J. Appl. Phys. **77**, 5518 (1995).
[13] P. A. Thielen, L. B. Shaw, P. C. Pureza, V. Q. Nguyen, J. S. Sanghera, I. D. Aggarwal, Optics Letters **28**, 1406 (2003).
[14] G. G. Devyatykh, M. F. Churbanov, I. V. Scripachev, E. M. Dianov, V. G. Plotnichenko, International Journal of Optoelectronics **7**, 237 (1992).
[15] G. Edwards, R. Logan, M. Copeland, L. Reinisch, J. Davidson, B. Johnson, R. Maciunas, M. Mendenhall, R. Ossoff, J. Tribble, J. Wekhaven, D. O'Day, Nature **371**, 416 (1994).
[16] P. A. Thielen, L. B. Shaw, J. S. Sanghera, I. D. Aggarwal, Optics Express **11**, 3248 (2003).
[17] L. B. Shaw, P. A. Thielen, F. H. Kung, V. Q. Nguyen, J. S. Sanghera, I. D. Aggarwal, IR supercontinuum generation in As-Se photonic crystal fiber, Proceedings of Advanced Solid State Photonics, TOPS vol. 98, Optical Society of America, 2005.
[18] E. M.Dianov, P. G. Kazansky, D. Yu. Stepanov, Sov. J. Quant. Electron. **19**, 575 (1989).
[19] M. T. De Aruajo, M. V. D. Vermelho, A. S. Gouveia-Net, A. S. B.Sombra, Medeiros Neto J.A., IEEE Photonics Technol. Letts. **8**, 821 (1996).
[20] P. G. Kazansky, P. S. J. Russell, H. Takabe, J. Lightwave Tech. **15**, 1484 (1997).
[21] A. B. Ruffin, "Stimulated Brillouin Scattering: An overview of measurements, system impairments, and applications", NIST Symposium on Optical Fiber Measurements, Technical Digest, 23 (2004).
[22] K. Y. Song, K. S. Abedin, K. Hotate, M. G. Herráez, L. Thévenaz, Opt. Expr. **14**, 5860 (2006).
[23] E. P. Ippen, R. H. Stolen, Appl. Phys. Lett. **21**, 539 (1972).
[24] K. Ogusu, H. Li, M. Kitao, J. Opt. Soc. Am. B **21**, 1302 (2004).
[25] K. Y. Song, M. G. Herráez, L. Thévenaz, Opt. Expr. **13**, 82 (2005).
[26] A. B. Ruffin, M-J Li, X. Chen, A. Kobyakov, F. Annunziata, Opt. Lett. **30**, 3123 (2005).
[27] C. Jáuregui, H. Ono, P. Petropoulos, D. J. Richardson, OFC, paper PDP2 (2006).
[28] J. H. Lee, T. Tanemura, K. Kikuchi, T. Nagashima, T. Hasegawa, S. Ohara, N. Sugimoto, Opt. Lett. **30**, 1698 (2005).

*Corresponding author: sanghera@ccs.nrl.navy.nil